TU Delft

Delft University of Technology

20-Fold Increased Limiting Currents in Oxygen Reduction with Cu-tmpa by Replacing Flow-By with Flow-Through Electrodes

Ligthart, Nathalie E.G.; van Langevelde, Phebe H.; Padding, Johan T.; Hetterscheid, Dennis G.H.; Vermaas, David A.

DOI
10.1021/acssuschemeng.4c03919

Publication date
2024

Document Version
Final published version

Published in
ACS Sustainable Chemistry and Engineering

Citation (APA)
Ligthart, N. E. G., van Langevelde, P. H., Padding, J. T., Hetterscheid, D. G. H., & Vermaas, D. A. (2024). 20-Fold Increased Limiting Currents in Oxygen Reduction with Cu-tmpa by Replacing Flow-By with Flow-Through Electrodes. *ACS Sustainable Chemistry and Engineering*, *12*(34), 12909-12918. https://doi.org/10.1021/acssuschemeng.4c03919

Important note
To cite this publication, please use the final published version (if applicable).
Please check the document version above.

Copyright
Other than for strictly personal use, it is not permitted to download, forward or distribute the text or part of it, without the consent of the author(s) and/or copyright holder(s), unless the work is under an open content license such as Creative Commons.

Takedown policy
Please contact us and provide details if you believe this document breaches copyrights.
We will remove access to the work immediately and investigate your claim.

This work is downloaded from Delft University of Technology.
For technical reasons the number of authors shown on this cover page is limited to a maximum of 10.

ACS Sustainable Chemistry & Engineering

pubs.acs.org/journal/ascecg

Open Access

This article is licensed under CC-BY 4.0

Research Article

20-Fold Increased Limiting Currents in Oxygen Reduction with Cu-tmpa by Replacing Flow-By with Flow-Through Electrodes

Nathalie E.G. Ligthart, Phebe H. van Langevelde, Johan T. Padding, Dennis G.H. Hetterscheid, and David A. Vermaas*

Cite This: *ACS Sustainable Chem. Eng.* 2024, 12, 12909−12918

Read Online

ACCESS | Metrics & More | Article Recommendations | Supporting Information

ABSTRACT: Electrochemical oxygen reduction is a promising and sustainable alternative to the current industrial production method for hydrogen peroxide (H_2O_2), which is a green oxidant in many (emerging) applications in the chemical industry, water treatment, and fuel cells. Low solubility of O_2 in water causes severe mass transfer limitations and loss of H_2O_2 selectivity at industrially relevant current densities, complicating the development of practical-scale electrochemical H_2O_2 synthesis systems. We tested a flow-by and flow-through configuration and suspension electrodes in an electrochemical flow cell to investigate the influence of electrode configuration and flow conditions on mass transfer and H_2O_2 production. We monitored the H_2O_2 production using Cu-tmpa (tmpa = tris(2-pyridylmethyl)amine) as a homogeneous copper-based catalyst in a pH-neutral phosphate buffer during 1 h of catalysis and estimated the limiting current density from CV scans. We achieve the highest H_2O_2 production and a 15−20 times higher geometrical limiting current density in the flow-through configuration compared to the flow-by configuration due to the increased surface area and foam structure that improved mass transfer. The activated carbon (AC) material in suspension electrodes, which have an even larger surface area, decomposes all produced H_2O_2 and proves unsuitable for H_2O_2 synthesis. Although the mass transfer limitations seem to be alleviated on the microscale in the flow-through system, the high O_2 consumption and H_2O_2 production cause challenges in maintaining the initially reached current density and Faradaic efficiency (FE). The decreasing ratio between the concentrations of the O_2 and H_2O_2 in the bulk electrolyte will likely pose a challenge when proceeding to larger systems with longer electrodes. Tuning the reactor design and operating conditions will be essential in maximizing the FE and current density.

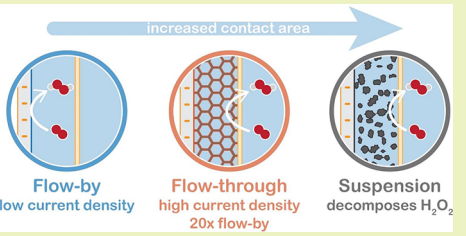

KEYWORDS: *hydrogen peroxide, electrolysis, oxygen reduction reaction, mass transfer, flow-through, cell design, flow chemistry*

Downloaded via TU DELFT on August 29, 2024 at 08:27:00 (UTC).
See https://pubs.acs.org/sharingguidelines for options on how to legitimately share published articles.

INTRODUCTION

Hydrogen peroxide (H_2O_2) is an important chemical that is widely used in established methods for chemical synthesis,[1] disinfection,[2] and bleaching,[3] as well as applications such as advanced oxidation processes in water treatment,[4] and fuel cells.[5] Contrary to the use of H_2O_2 as a green oxidant, its anthraquinone production process is energy-intensive and environmentally unfriendly.[6] The continued and increasing demand[7] for H_2O_2 as a green oxidant has provoked the development of alternative production methods, such as electrochemical 2e$^-$ oxygen (O_2) reduction.

The oxygen reduction reaction (ORR) can run on renewable energy, water, and oxygen as inputs and provides a sustainable route for H_2O_2 synthesis,[8] but suffers from challenges imposed by the low solubility of O_2 in water (1.1 mM when in contact with pure O_2 gas at standard conditions). The small amount of O_2 available near the electrode depletes rapidly when working at higher current densities. This causes severe mass transfer limitations and lowers catalyst selectivity considerably at economically viable current densities.[9,10] Electrochemical H_2O_2 synthesis has been commercialized in the Dow-Huron process[11] that produces highly alkaline H_2O_2 solutions, of which the pH is lowered after production to prevent H_2O_2 decomposition and to fit the requirement for acidic or neutral H_2O_2 solutions of many applications. Commercially applicable processes for producing neutral and acidic H_2O_2 solutions directly are still lacking.[12] Improved reactor designs are necessary to alleviate mass transfer limitations and advance toward widely applicable practical-scale electrochemical H_2O_2 synthesis devices.[5]

Here, we perform ORR in an electrochemical flow cell with three different electrode configurations and Cu-tmpa (tmpa = tris(2-pyridylmethyl)amine) as the catalyst. This catalyst was selected because it is the fastest copper-based molecular ORR catalyst reported to date, catalyzing the reduction of oxygen with more than 2 million turnovers per second.[13] Furthermore, electrochemical experiments have shown that this Cu-based

Received: May 12, 2024
Revised: July 27, 2024
Accepted: July 29, 2024
Published: August 12, 2024

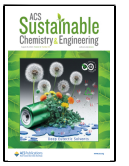

© 2024 The Authors. Published by American Chemical Society

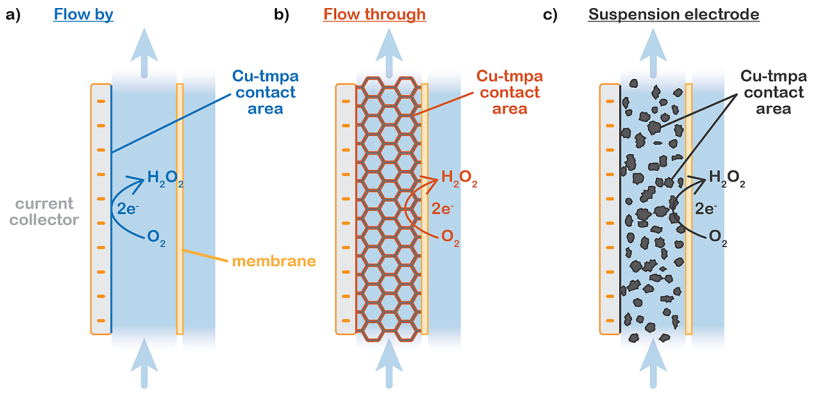

Figure 1. Studied current collector configurations (a) flow-by, (b) flow-through, and (c) suspension electrodes, for homogeneous catalysis of oxygen reduction by Cu-tmpa.

molecular catalyst converts O_2 in neutral pH in two consecutive steps, starting with a fast 2-electron reduction of O_2 to H_2O_2, followed by a slower second 2-electron reduction of H_2O_2 to H_2O, therefore generating H_2O_2 as a stable intermediate.[13,14] It has been shown that in a rotating disk electrode (RDE) setup, the ORR selectivity is determined by the local O_2 and H_2O_2 concentrations at the electrode surface, and thus highly dependent on transport of O_2 toward and H_2O_2 away from the electrode.[15] Cu-tmpa was shown to generate H_2O_2 solutions with high Faradaic efficiency (FE) for up to 8 h. However, an RDE setup is a highly controlled and idealized system. Therefore, in this work, we extend Cu-tmpa studies that have been limited to fundamental studies on RDEs to more applicable flow systems with a larger electrode area to obtain insight into the effect of cell configuration on the activity and selectivity of H_2O_2-generating molecular catalysts. Additionally, we study the influence of the different electrode configurations and electrolyte flow velocities on mass transfer-limited electroconversion, and we relate our findings to the implications for larger electrodes to provide insights helpful for scaling up electrochemical H_2O_2-generating systems.

Replacing 2D electrodes by 3D structures can alleviate mass transfer limitations by providing a larger contact area with the electrolyte and shorter mass transport distances.[10,16] We perform the ORR in a conventional flow-by configuration (2D), as well as in a flow-through configuration and on a flowing suspension electrode (both 3D). The flow-by configuration consists of a flat electrode with the electrolyte flowing along its surface (Figure 1a), and it is likely to develop a thick diffusion boundary layer and severe mass transfer limitations. The flow-through configuration has an electrically conductive foam inserted into the electrolyte flow path (Figure 1b), enlarging the contact area, allowing the electric current to percolate through the entire channel, and hindering the development of a thick boundary layer. The suspension electrode is composed of conductive porous microparticles suspended in an electrolyte and flows along a 2D current collector (Figure 1c). The porous particles provide an even larger surface area than the foam, while conductive networks and particle collisions also allow for electron percolation into the channel.[17−19]

Evaluating the influence of reactor design on mass transfer is essential for achieving the high product selectivity and current densities needed for advancing electrochemical H_2O_2 synthesis to an industrially relevant technology.

METHODS

Cu-tmpa was synthesized as described by Langerman et al.[14] All experiments were performed in the electrochemical flow cell and setup shown in Figure S1. The cathodic and anodic compartments (3 mm thick) were separated by a Nafion 117 cation exchange membrane (CEM) that was soaked and stored in an electrolyte. We used a three-electrode setup, with a glassy carbon plate (Goodfellow) used as cathodic current collector in all experiments, of which an area of 2.4 × 3.4 cm was exposed to the electrolyte. This was combined with a vitreous carbon foam (3.2 mm thickness, 24 pores/cm, 96.5% porosity, surface area 3937 m^2/m^3, Goodfellow) cut into the same dimension and inserted into the flow channel to create the flow-through configuration. An Ir-/Ru-oxide coated Ti-sheet (Permascand) was used as the anode. A leak-free Ag/AgCl electrode (LF-1-45, Alvatek) was used as a reference electrode (RE). It was inserted through the side of the flow channel with its tip in front of the glassy carbon plate, as illustrated in Figure S1. A small hole (Ø 3 mm) was made in the carbon foam at this spot to accommodate for the RE insertion.

A phosphate buffer of 0.5 M Na_2HPO_4/NaH_2PO_4 (≥99.999%, Honeywell Fluka TraceSELECT) at pH 7 was used as catholyte and anolyte to allow for comparison with previous studies,[13−15] and to provide good Cu-tmpa and H_2O_2 stability and sufficient conductivity to achieve acceptable cell potentials. The catholyte was saturated with oxygen by sparging O_2 gas at 50 mL/min (controlled with mass flow controllers by Bronckhorst) during and for at least 30 min before the experiment. 80 mL of catholyte and anolyte were used in the case of the flow-by and flow-through configurations, 40 g of carbon suspension in 0.5 M phosphate buffer replaced the catholyte, and 40 mL of phosphate buffer was used as anolyte in the suspension electrode experiments. The suspension was prepared by adding 10 or 20 wt % of activated carbon (AC, 20 μm median particle size, 1000 m^2/g, Norit SX Plus CAT, Sigma-Aldrich) to the phosphate buffer under thorough stirring, followed by 30 min of sonication.

Cyclic voltammetry scans (CVs) were performed at a scan rate of 100 mV/s using an IviumStat (±5 A/±10 V, Ivium) potentiostat (see the Supporting Information for more details). The scans were performed at various flow speeds (peristaltic pump, L/S Precision Pump System, Masterflex) before and between two additions of 5 μM Cu-tmpa to investigate the effect of flow and catalyst concentration on the limiting current.

The ORR performance was evaluated during chronoamperometry (CA) at a cathode potential close to the half-wave potential ($E_{cat/2}$) of 0.3 vs RHE found in previous studies[13,14] that results in roughly 75% of the peak current. This allowed us to push the current densities toward their maximum without entering the mass transfer-limited regime in the CVs. As the catalytic peaks were not visible in the CV scans of the suspension electrodes, the suspension CAs were run at the potentials selected for the flow-by and flow-through configurations. Each CA was run for 1 h at a flow velocity inside the catholyte channel of 19 mm/s when using the flow-by and flow-

https://doi.org/10.1021/acssuschemeng.4c03919
ACS Sustainable Chem. Eng. 2024, 12, 12909−12918

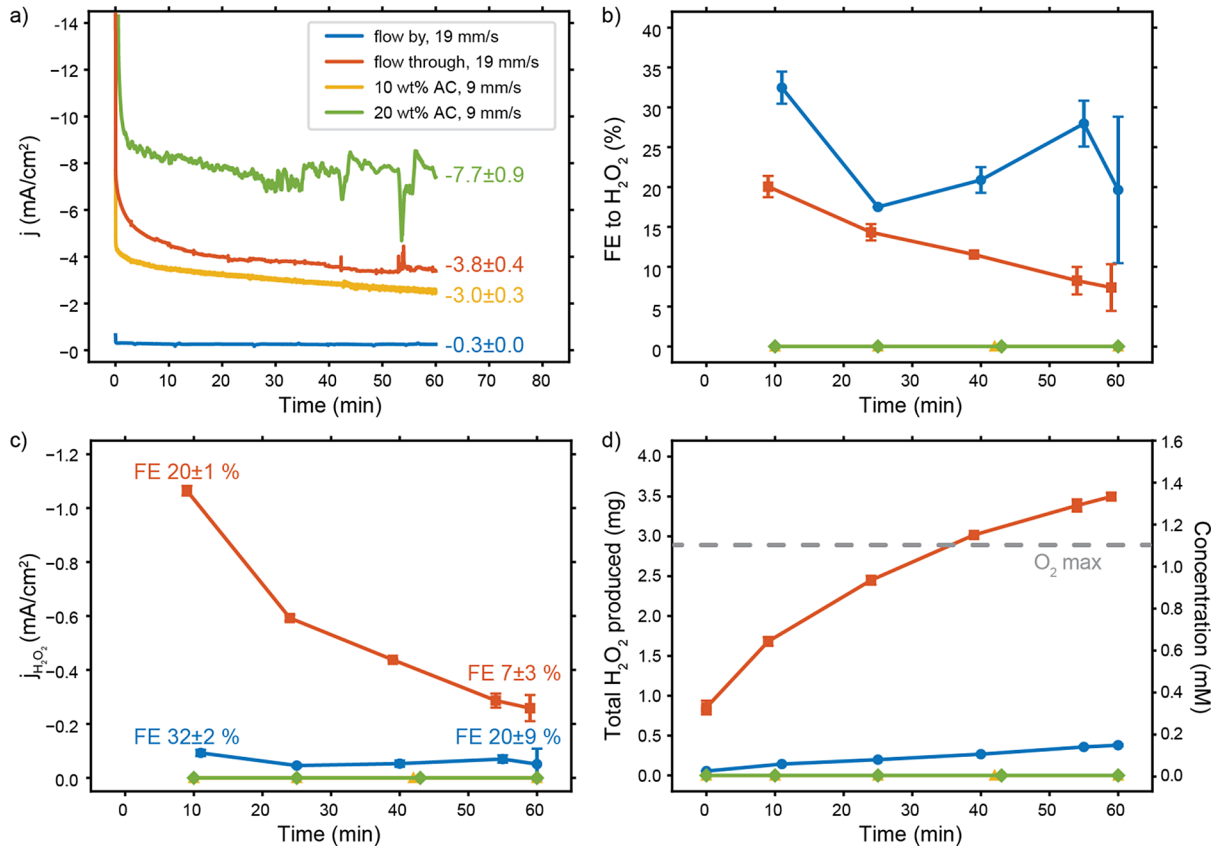

Figure 2. Overall performance of O_2 reduction by 10 μM Cu-tmpa in 0.5 M phosphate buffer (pH 7) on flow-through, flow-by, and suspension (10 and 20 wt % AC) electrodes. (a) Chronoamperometry showing the differences in achieved current densities through time, performed at 0.31 V vs RHE for the flow-by and 10 wt % suspension, and 0.21 V vs RHE for the flow-through and 20 wt % suspension. The 20 wt % AC graph has been smoothed through a running average over 30 s to remove excessive noise. (b) Measured FE toward H_2O_2 production, and (c) achieved partial current density to H_2O_2 ($j_{H_2O_2}$) through time. (d) Resulting cumulative H_2O_2 production over time in mg and mM. The H_2O_2 concentration exceeds the maximum O_2 concentration after 36 min of operation in the flow-through configuration.

through configurations, and at a lower flow velocity of 9 mm/s when using a suspension electrode to prevent operational complications such as clogging over the course of the experiment. The H_2O_2 concentration was measured periodically with a reflectometer (RQflex 20, Merck) and corresponding peroxide test strips (0.2−20.0 mg/L H_2O_2). The accuracy of the test strips for measuring peroxide has been verified in ref.[15] The samples were diluted with a buffer to fit the detection window of the test strips whenever necessary. The precise reaction conditions of each experiment are listed in Table S1.

The stability of H_2O_2 in the different experimental conditions was tested by adding a known amount of H_2O_2 and measuring the concentration in the liquid at time intervals. In the case of the flow-by and flow-through configurations, the flow cell was assembled as described above. The anolyte compartment was filled with electrolyte and closed off, while 72 g of buffer was cycled through the catholyte compartment at 40 mL/min (9 mm/s inside the channel). In the case of the suspension electrode, the H_2O_2 concentration was monitored after addition to 80 g of the 10 wt % AC suspension under continuous stirring inside a glass bottle. The first sample was taken 30 s after each addition and passed through a filter (Whatman Puradisc H-PTFE syringe filters, 0.2 μm, hydrophilic) to remove the AC before measuring the H_2O_2 concentration with the reflectometer. Taking the sample and filtering took about 10 min.

A similar experiment was performed to investigate whether H_2O_2 was decomposed or adsorbed by the AC particles. Known amounts of H_2O_2 were injected into the 10 wt % AC suspension inside a gastight bottle, and gas samples were taken and analyzed with a gas chromatograph (GC, CompactGC4.0, Interscience) to track O_2 evolution.

RESULTS AND DISCUSSION

Flow-Through Configuration Improves the H_2O_2 Production. We measured the current density of the ORR and concentration of produced H_2O_2 in the electrolyte during 1 h of CA for comparison of the electrochemical performance in each configuration. Figure 2a shows a significant difference in the achieved current densities among the different configurations, with the 20 wt % AC suspension reaching the highest current density of -7.7 ± 0.9 mA/cm^2, about twice the current density reached in the 10 wt % AC suspension (-3.0 ± 0.3 mA/cm^2) and the flow-through electrode (-3.8 ± 0.4 mA/cm^2), and almost 26 times higher than the flow-by configuration, which reaches only -0.3 ± 0.0 mA/cm^2.

In addition, we observe a steady decrease in the current density in all systems during CA, especially those operating at higher current densities. The FE decreases over time as well, in the flow-by and flow-through configurations (Figure 2b). Both effects decrease the H_2O_2 formation rate over time. We suspect that this is due to two complications. First, the decrease in selectivity over time can be caused by the increasing concentration of H_2O_2, both in the reservoir and through the height of the cell, leading to increased Faradaic over-reduction of the produced H_2O_2 to form H_2O and resulting in a lower measured FE toward H_2O_2. This is especially an issue in the flow-through configuration, in which the H_2O_2 concentration increases most severely and even exceeds the

https://doi.org/10.1021/acssuschemeng.4c03919
ACS Sustainable Chem. Eng. 2024, 12, 12909−12918

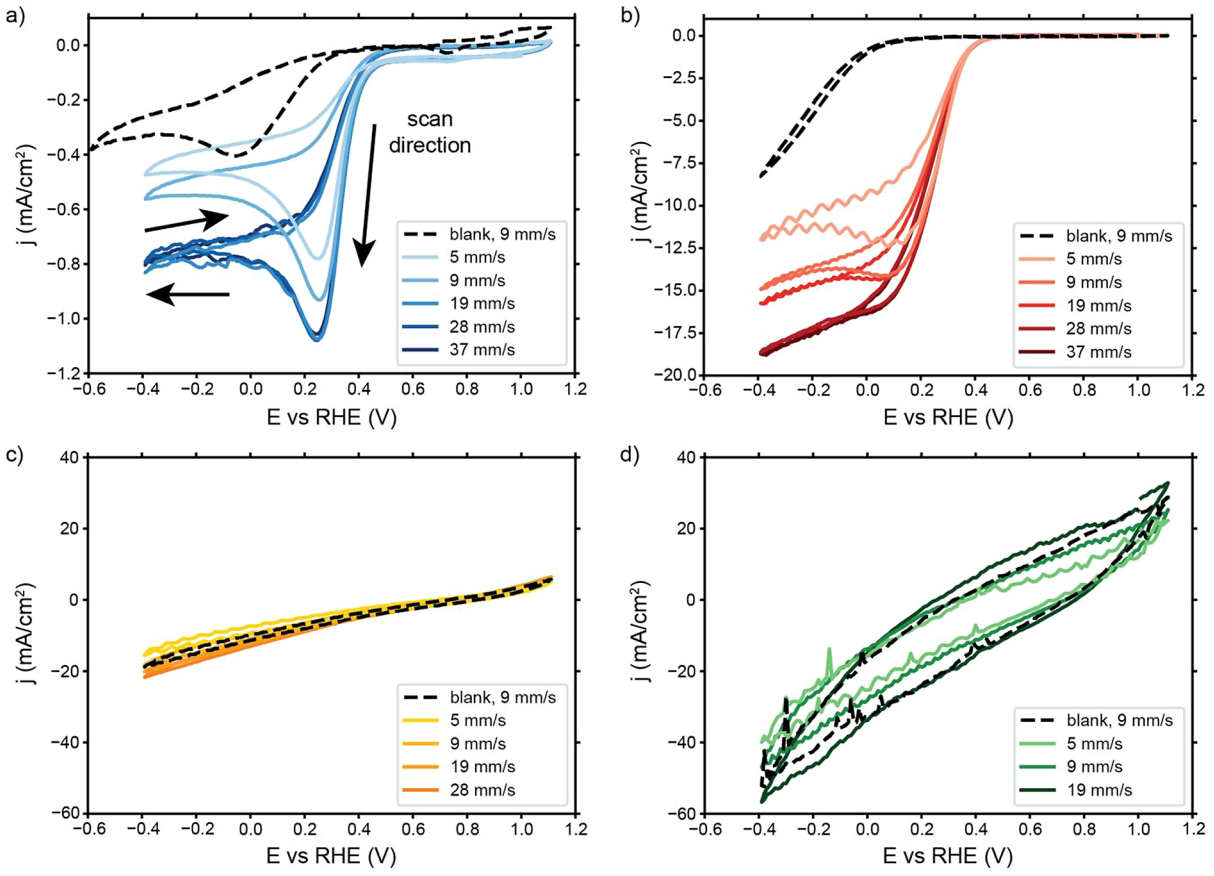

Figure 3. CV scans of 5 μM Cu-tmpa in O_2-saturated 0.5 M phosphate buffer of pH 7 under various flow velocities with (a) glassy carbon plate (flow-by), (b) glassy carbon foam (flow-through), (c) 10 wt % AC suspension, and (d) 20 wt % AC suspension electrodes, at a scan rate of 100 mV/s. The black dashed lines correspond to blank measurements without any Cu-tmpa present. The blank measurement in the flow-by shows an extra reduction peak at an earlier onset potential or ORR on glassy carbon than in the flow-through configuration due to a contaminant. Nevertheless, addition of Cu-tmpa clearly increases the current and decreases the onset potential in the flow-by and flow-through systems but not in the suspensions. Current fluctuations are visible in some scans; we suspect these are caused by the pulsed flow from the peristaltic pump.

O_2 concentration after about 36 min of operation, as shown in Figure 2d. While such concentrations generally do not lead to a loss in FE when using an RDE,[15] H_2O_2 accumulation has been shown to decrease selectivity in flow cells.[20] The produced H_2O_2 spends a significantly longer time near the electrode before getting diluted inside the reservoir, compared to a setup using an RDE. This essentially increases the risk of H_2O_2 reduction. Second, the overall decrease in current density over time can be caused by slow dissolution of O_2 in the reservoir. To illustrate, all dissolved O_2 will be consumed within 9 min at the ORR rate reached in the flow-through configuration if no fresh O_2 is supplied (see Supporting Information for calculation). Reaching a sufficiently high dissolution rate to keep up with the O_2 consumption and maintain the maximum O_2 concentration is challenging and unlikely when using a simple sparger for saturation.[10] Both the O_2 depletion and H_2O_2 accumulation contribute to altering the O_2/H_2O_2 ratio near the electrode and affect the ORR and the hydrogen peroxide reduction reaction (HPRR) rates according to the ORR rate = k_{ORR}[Cu-tmpa][O_2] and HPRR rate = k_{HPRR}[Cu-tmpa][H_2O_2], increasing the HPRR rate during the CA. In turn, this also lowers the overall current density because k_{HPRR} is an order of magnitude lower than k_{ORR}.[13] The combination of these two effects ultimately leads to a more severe loss in partial H_2O_2 current density in the flow-through than in the flow-by case (Figure 2c).

Despite the lower selectivity, the flow-through configuration displays the highest partial H_2O_2 current density at all times (Figure 2c). The higher H_2O_2 production rate results in almost 10 times more H_2O_2 being produced in the flow-through configuration than in the flow-by configuration within 1 h of operation (Figure 2d). The flow-through setup produces concentrations in the mM range, which is already sufficiently high for applications like H_2O_2/UV disinfection.[21]

Although the total current densities achieved in the suspension electrodes almost match (for 10 wt % AC) or even surpass (for 20 wt % AC) the total current density reached in the flow-through configuration, no H_2O_2 was detected in the suspensions. We suspect that the suspensions are interfering negatively with the reaction because the glassy carbon plate used in the flow-by system is also present here and was expected to allow for at least some H_2O_2 production. We will address this issue later.

Electrode Configuration and Flow Conditions Enhance Mass Transfer. We performed CV scans to further study what current densities can be reached in our H_2O_2 synthesis systems and how this relates to the applied potential and the electrolyte flow rate. The CV scans for the different electrodes and flow velocities are shown in Figure 3. The current increases most sharply between roughly 0.4 and 0.2 V vs RHE, depending on the configuration. This is in line with

https://doi.org/10.1021/acssuschemeng.4c03919
ACS Sustainable Chem. Eng. 2024, 12, 12909−12918

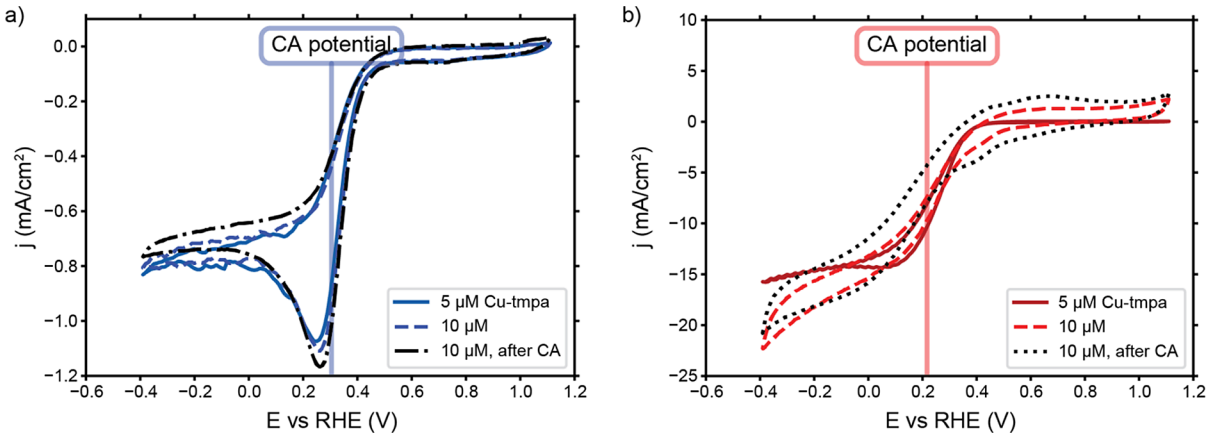

Figure 4. Influence of Cu-tmpa concentration and 1 h of chronoamperometry (CA) on CV scans at a scan rate of 100 mV/s and an electrolyte flow velocity of 19 mm/s with a (a) glassy carbon plate (flow-by) and (b) glassy carbon foam (flow-through) as current collectors. The vertical line indicates the potential applied during CA.

previous studies, wherein the half-wave potential ($E_{cat/2}$) was found at 0.3 V vs RHE.[13,14]

First we consider the CVs of the flow-by (Figure 3a) and flow-through (Figure 3b) cases. The flow-by configuration leads to a typical peak-shaped CV with a peak current in the forward scan caused by the transition from saturated O_2 conditions at the electrode surface to the formation of a depleted diffusion boundary layer. The peak is followed by a plateau toward the cathodic vertex, where the O_2 at the surface has already been depleted and the current is limited by O_2 transport from the freshly delivered bulk electrolyte. Increasing the flow velocity increases the peak current and plateau current to a certain extent by lowering the residence time and reducing the boundary layer thickness, respectively.

The flow-through configuration (Figure 3b) reaches a significantly higher geometrical current density of 5−15 times, depending on the flow rate, compared to the highest peak current in the flow-by configuration (Figure 3a). The active surface area per flow cell area is increased 13.5 times by the porosity of the flow-through electrode compared to the flow-by plate electrode (see Supporting Information for calculation). This suggests that most of the increase in the geometric current density is due to the larger active surface area. However, the difference in CV shape reveals that the mass transfer conditions also depend on the electrode systems. The lowest flow velocity (5 mm/s) for flow-through results in a similar shape as we have seen in the flow-by configuration but with a less pronounced peak at 0.25 V. The peak shape transforms to resemble an S-shape voltammogram with increasing flow velocity and is completely invisible when applying higher flow velocities (28 and 37 mm/s). The plateau shape in the CV indicates that a constant O_2 supply is available, which corresponds with O_2 transport from the bulk instead of O_2 from a transient boundary layer build-up. The transition toward steady-state diffusion (S-shape) at relatively low flow velocities suggests that the boundary layer in the flow-through is much thinner than in the flow-by case. This makes sense, as the 3D character of the foam forces a frequent restart of the boundary layer development along the length of the channel. Therefore, the foam reduces the boundary layer thickness compared to the flow-by system, in which the diffusion boundary layer continues to develop along the entire channel length, resulting in an ever-increasing boundary layer thickness along the current collector surface. We estimate the average boundary layer thickness (δ) in the flow-by configuration at 180 μm, versus 11 μm in the flow-through configuration, using $\delta = \frac{D}{k}$, with D the diffusion coefficient of O_2 in water, and k the mass transfer coefficient.[22,23] We obtain the mass transfer coefficients of a plate and foam, k_{plate} and k_{foam}, respectively, later with eqs 3−5.

Although suspension electrodes give even higher current densities compared with the flow-by and flow-through configurations (Figure 3c,d), the ORR performance cannot be compared from these scans. The steep slope of the ORR that is expected below 0.6 V vs RHE is clearly present in the other flow configurations but is not visible when using the suspension electrodes, and we do not see a difference between the experiments in the presence or absence of catalyst. The high currents seem to be due to the high capacitance of the suspensions, caused by the large surface area of the porous carbon particles. This agrees with the increase in hysteresis when comparing the 10 wt % (Figure 3c) with the 20 wt % (Figure 3d) AC suspension, as the increase in carbon loading raises the capacitance for two reasons: (1) a higher carbon loading results in a larger surface area, and (2) a higher carbon loading also gives higher conductivity and more percolation into the bulk of the electrode, making more surface area accessible for capacitive charging.[24] The large capacitance of the suspensions makes it impossible to observe an onset potential for the ORR in CVs and shows that at least part of the current during CA can be attributed to electric double layer (EDL) charging.

Catalyst Concentration and Stability. We performed CVs with Cu-tmpa concentrations of 5 and 10 μM to check whether the current is limited by catalyst availability in addition to O_2 availability. Doubling the Cu-tmpa concentration had no significant effect on the reached currents in any of the configurations, as shown in Figure 4a,b for the flow-by and flow-through configurations, respectively (see Supporting Information for the suspensions). This is in line with observations inside this concentration range in RDE systems.[15] The altered shape of the scans performed on the flow-through with 5 versus 10 μM Cu-tmpa was caused by a short contact loss of the RE while scanning the positive potentials, etching the foam surface, and causing a larger EDL to become visible in the CVs. The potential range of interest remained

https://doi.org/10.1021/acssuschemeng.4c03919
ACS Sustainable Chem. Eng. 2024, 12, 12909−12918

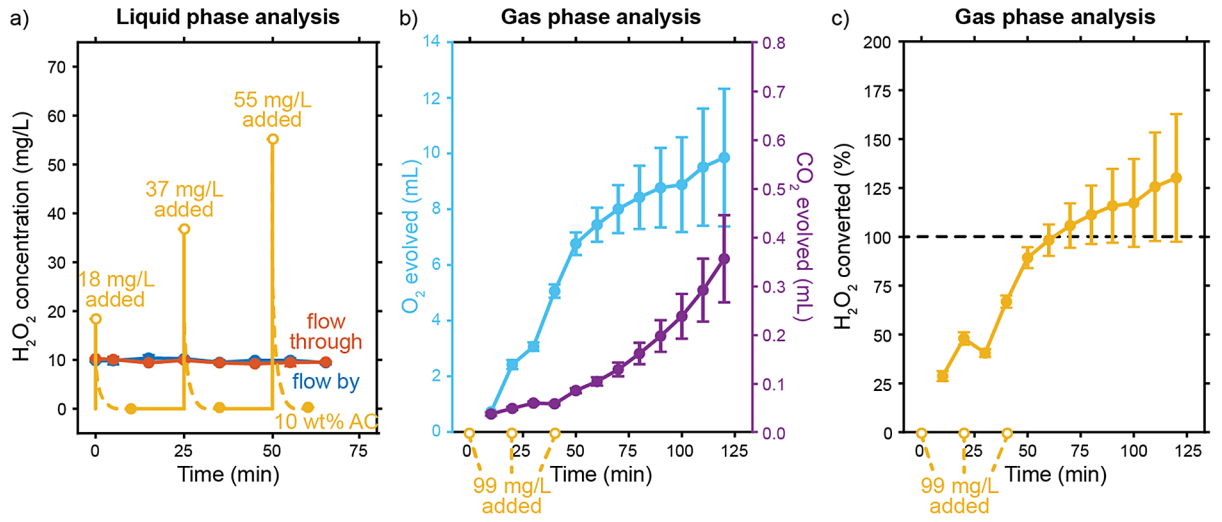

Figure 5. Results showing the 10 wt % activated carbon (AC) suspension breaking down H_2O_2 in solution. (a) Measured H_2O_2 concentrations through time after one addition of 10 mg/L H_2O_2 in case of the flow-by, flow-through case, and after additions of 18, 37, and 55 mg/L H_2O_2 to the 10 wt % AC suspension case, spaced 25 min apart. H_2O_2 disappears before the concentration in the liquid phase of the suspension can be measured. (b) O_2 evolution through time after adding H_2O_2 to the 10 wt % AC suspension. Smaller amounts of CO_2 evolve, as well. (c) Percentage of the H_2O_2 added that has been decomposed by the 10 wt % AC suspension, as calculated from the evolution of the O_2 through time.

unaffected, and we conclude that neither system is limited by the low Cu-tmpa concentration.

In addition, we performed CVs after 1 h of catalysis ("after CA" curves in Figure 4) at the indicated CA potentials to check the catalyst stability. The shape and reached currents are very similar to those before the CA, suggesting that loss of catalytic activity or Cu-tmpa degradation is not likely cause for the FE loss through time observed in Figure 2. Cu-tmpa reached a turnover number (TON) of 130 during the experiments, which is likely considerably lower than the maximum TON Cu-tmpa can reach in catalysis of the ORR. Previous studies have shown that a TON of at least 250 is achievable.[15] However, very subtle differences can be observed in the CVs. The slight increase in slope in the flow-by configuration is caused by an increase in the available reactant in the form of H_2O_2, and the slight broadening of the flow-through CV can indicate further etching of the foam surface during additional CVs before catalysis. The suspension CVs (Figure S2) show a decrease in current after catalysis, which is in line with the capacitive nature of the suspensions and our observations from Figure 3c,d.

AC Suspensions Break Down H_2O_2. Even though the AC suspensions show a non-Faradaic response due to their large capacitance, the applied potential was equal to the flow-by and flow-through cases and sufficient for catalysis of the ORR. However, we did not detect any H_2O_2 production when applying a potential for a long period of time (Figure 2). To investigate this further, we studied the stability of H_2O_2 in a stirred suspension of 10 wt % AC without a potential applied. We added known concentrations of H_2O_2 to the suspension and measured the concentration in the electrolyte within 10 min after each addition (Figure 5a). No H_2O_2 was detectable in any of these measurements, showing that it vanishes rapidly after addition to an AC suspension via a non-Faradaic process. In contrast, no H_2O_2 loss was observed while pumping an electrolyte with known H_2O_2 concentrations through the flow-by and flow-through configurations.

We performed the same experiment in a gastight bottle and analyzed the evolving gases to determine whether the suspension decomposes or adsorbs the added H_2O_2 on its large surface area. Gas-phase analysis showed the formation of significant amounts of O_2 upon addition of H_2O_2 to the suspensions (Figure 5b). This shows that the H_2O_2 disproportionates on the AC particles via $2\ H_2O_2 \rightarrow 2\ H_2O + O_2$. Figure 5c shows how much of the added H_2O_2 has decomposed over time and that the AC particles can break down all added H_2O_2 within 2 h. Note that the concentration added in this experiment is 6 times higher than the eventual concentration formed in 1 h of catalysis in the flow-through configuration, according to Figure 2. In addition, we also detected smaller amounts of CO_2 forming, which can indicate the oxidation of the carbon particles by H_2O_2.

Hence, we have shown that the AC suspensions would decompose any H_2O_2 produced by the ORR through non-Faradaic disproportionation, in addition to the already competing Faradaic HPRR. The fast H_2O_2 decay prevents us from monitoring how much is produced in the suspension electrodes during CA (Figure 2a). Although the suspension electrodes rival (10 wt % AC) and even surpass (20 wt % AC) the flow-through configuration in terms of achieved total current density, we conclude that either no H_2O_2 was produced on the suspension electrodes, or any produced H_2O_2 was rapidly decomposed on the suspension particles' large surface area. Therefore, the AC particles used in this study are not suitable for use in H_2O_2 production systems. As a result, the envisaged advantages of using the suspension electrode configuration depicted in Figure 1c could not be realized in this work.

Nevertheless, carbon-based ORR catalysts have been studied extensively in literature and are considered to have great prospects.[8,25] Suspensions of carefully selected carbon materials may not exhibit the issues we encounter here. Materials such as carbon black (CB), carbon nanotubes (CNTs), and graphene-based materials are commonly used in suspension electrodes,[17,26,27] and can be modified to act as ORR catalyst[8,9] as well. Such modified CB, CNT, and graphene-based materials would be promising to test as suspension electrodes for H_2O_2 production. Alternatively, a

https://doi.org/10.1021/acssuschemeng.4c03919
ACS Sustainable Chem. Eng. 2024, 12, 12909−12918

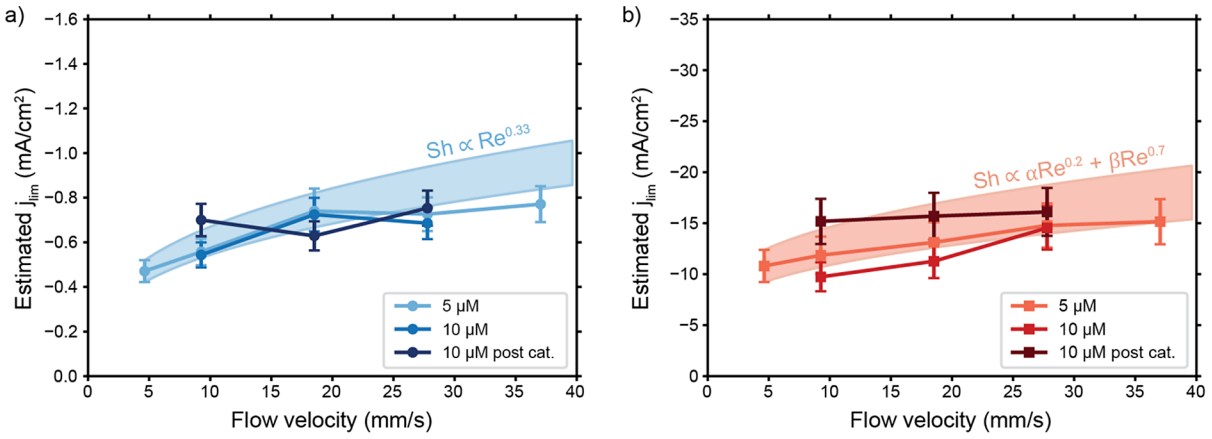

Figure 6. Estimated current densities in the (a) flow-by and (b) flow-through configurations at various flow velocities and catalyst concentrations obtained from CV measurements recorded before and after 1 h of chronoamperometry. Our method for estimating the limiting current densities and the errors is included in the Supporting Information. The shaded areas indicate the expected increase in j_{lim} of the 5 μM line with flow velocity based on Sh $\propto$ Re$^{0.33}$ and Sh $\propto \alpha$Re$^{0.2}$ + βRe$^{0.7}$ as indicated.

small amount of flowing carbon-based catalyst can be used in combination with a conductive foam to replicate the flow-through configuration with a heterogeneous catalyst instead of Cu-tmpa.

Comparing Limiting Current Densities to Sherwood Correlations. Having established that a flow-through electrode offers a major advantage in mass transport compared to flow-by electrodes, we can further study the physical cause of the higher limiting current densities. The electrolyte flow velocity and channel properties influence the limiting current density (j_{lim}) of a mass transfer limited reaction through the Sherwood number (Sh). A higher Sherwood number represents an increased mass transfer coefficient (k) and a decreased diffusion boundary layer thickness (δ), leading to a higher limiting current density through eqs 1−3,[22,23]

$$j_{lim} = \frac{DnFc_{bulk}}{\delta} \tag{1}$$

$$\delta = \frac{D}{k} \tag{2}$$

$$k = \frac{ShD}{d_c} \tag{3}$$

in which D is the diffusion coefficient, n the number of electrons involved in the reaction, F the Faraday constant, c_{bulk} the reactant concentration outside the diffusion boundary layer, and d_c the characteristic length.

The Sherwood number along a planar electrode in laminar flow with a fully developed hydrodynamic boundary layer is given by[23]

$$\begin{aligned} Sh &= 1.467\left(\frac{2}{1+\gamma}\right)^{0.33}\left(ReSc\frac{d_h}{L}\right)^{0.33};\ \gamma \\ &= \frac{B}{L};\ d_h \\ &= 2BW(B+W) \end{aligned} \tag{4}$$

in which γ is the aspect ratio of the electrode, and d_h is the hydrodynamic diameter of the channel. These are determined by the electrode length (L), electrode and channel breadth (B), and channel depth (W). The Sherwood number of flow-through of a porous electrode can be estimated with[28]

$$\begin{aligned} Sh = {} & (7 - 10\varepsilon + 5\varepsilon^2)(1 + 0.7Re^{0.2}Sc^{0.33}) \\ & + (1.33 - 2.4\varepsilon + 1.2\varepsilon^2)Re^{0.7}Sc^{0.33} \end{aligned} \tag{5}$$

where ε is the porosity. Both expressions make use of the Reynolds (Re) and Schmidt (Sc) numbers, given by eqs 6 and 7, respectively.

$$Re = \frac{ud_c}{\nu} \tag{6}$$

$$Sc = \frac{\nu}{D} \tag{7}$$

which include the following equations: (a) the superficial flow velocity (u), the kinematic viscosity (ν) of the electrolyte, and a characteristic length scale d_c. The value of d_c is defined as d_h (hydrodynamic diameter) for the flow-by configuration and d_s (typical strut size) for the flow-through electrode. We use eqs 4 and 5 to obtain the Sherwood numbers at relevant flow velocities in the flow-by and flow-through configurations, respectively. The only flow rate-dependent term in both equations is the Reynolds number, so we expect Sh $\propto$ Re$^{0.33}$ in the flow-by electrode and approximately Sh $\propto \alpha$Re$^{0.2}$ + βRe$^{0.7}$ in the flow-through electrode. Figure 6 shows the limiting current density at various flow velocities as estimated from CV scans (see Supporting Information for the method). We compare the experimental results with the limiting current densities expected from the obtained Sherwood numbers via

$$Sh = \frac{d_c}{D}k = \frac{d_c}{D}\frac{j_{lim}}{nFc_{bulk}} = a \times j_{lim} \tag{8}$$

by fitting them to the limiting current density in the 5 μM Cu-tmpa solution at the lowest flow velocity (5 mm/s) via the factor a. The shaded areas in Figure 6 indicate the expected limiting current densities. Both configurations follow the predicted trends with Sh $\propto$ Re$^{0.33}$ and Sh $\propto \alpha$Re$^{0.2}$ + βRe$^{0.7}$ quite well. For the flow-through case, the dominance of the first term ($\alpha \approx 15.3\beta$) gives a weaker flow rate-dependence of approximately Sh $\propto \alpha$Re$^{0.2}$ in the low Re laminar flow regime compared to the flow-by electrode. The flow-by electrode benefits more from increased flow because of the severe diffusion boundary layer development over the electrode length, while the flow-through electrode keeps a thinner

https://doi.org/10.1021/acssuschemeng.4c03919
ACS Sustainable Chem. Eng. 2024, 12, 12909−12918

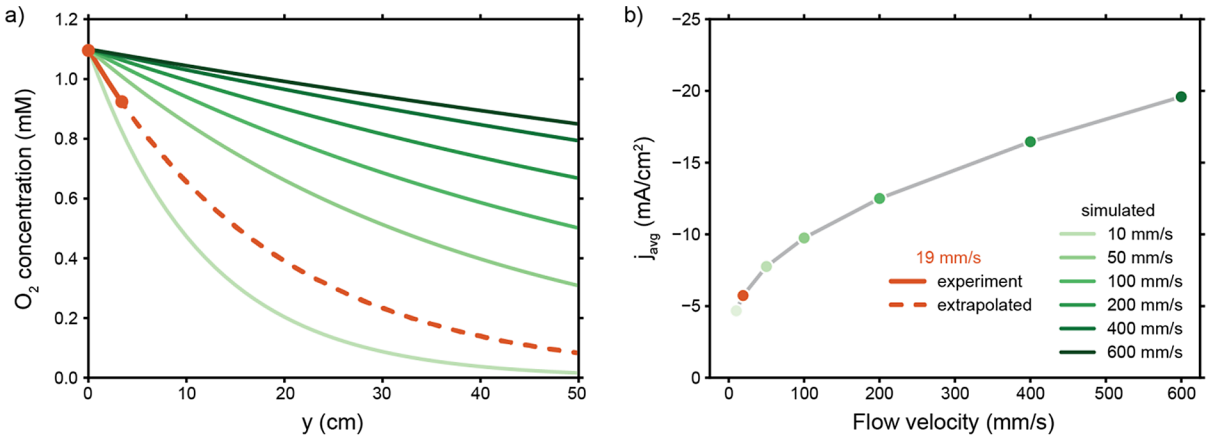

Figure 7. (a) Estimated O_2 concentration along the height of the flow cell at various flow velocities (see legend in b). (b) Average current density over a 50 cm long electrode at various flow velocities. Both estimates are based on Sherwood numbers and the average geometric current density of 5.7 mA/cm^2 during the first 5 min of catalysis on a 3.4 cm long electrode.

boundary layer already at low flow velocities because of the shorter developing lengths along the individual struts.

The second term of eq 5, for the flow-through electrode, will get larger than the first term when the Reynolds number exceeds 234, which mitigates the flattening of the curve. This situation is unlikely to occur in channels with dimensions that are typically used in electrolyzers. To illustrate, flow velocities of 5−40 mm/s give Reynolds numbers of only 1−8 in our flow cell. The threshold for Re can be lowered by using a flow-through electrode with lower porosity, but that will add to the pressure drop and pumping costs, as will increasing the flow rate.

Overall, we have shown that the type of current collector configuration (flow-by versus flow-through) can be used to boost the limiting current 15−25 times (see Figure S5). The current density can be raised further by increasing the flow velocity, and the achieved improvement fits well with our expectations from Sherwood correlations. However, flowing faster boosts the limiting current to a much smaller extent than does the electrode shape. Therefore, changing the electrode design is more effective than changing the flow rate.

Implications for Scale Up. Although the flow-through configuration alleviates mass transfer limitations on the microscale, the low amount of O_2 available in the bulk of the electrolyte can pose an issue through depletion of the O_2 along the height of the cell, especially when extrapolating to larger electrolyzers. The local current density is dependent on the local O_2 concentration and will thus decrease along the height of the channel as O_2 is consumed and the bulk concentration decreases. We derive the O_2 concentration profile from the microscopic mass balance (derivation available in the Supporting Information, Section 4.2), which results in

$$c(x) = c_0 e^{-kA_V x/u} \tag{9}$$

in which c_0 is the inlet concentration, and $A_V$is the specific surface area of the foam. The local geometric current density is given by

$$j_{loc}(x) = nFkA_V c(x)W = nFkA_V W c_0 e^{-kA_V x/u} \tag{10}$$

and can be integrated along the electrode length to yield the average geometric current density (j_{avg})

$$j_{avg} = \frac{nFWc_0 u}{L}(1 - e^{-kA_V L/u}) \tag{11}$$

We use eq 11 to extract an experimental mass transfer coefficient ($k_{u=0.019}^{exp}$) at a flow velocity of 19 mm/s by inserting the average achieved current density over the first 5 min of CA. We estimate the mass transfer coefficient for various flow velocities by multiplying the theoretical mass transfer coefficient (k^{th}), obtained from eqs 3 and 5, with a factor $k_{u=0.019}^{exp}/k_{u=0.019}^{th}$ to correct for the discrepancy between theory and our experimental setup.

We evaluate a system with an FE for the ORR of 100%, and we study the influence of flow velocity on the local O_2 concentration and the resulting average geometric current density. We calculate the concentration profile with eq 9 (Figure 7a) along the 3.4 cm long flow-through electrode (solid orange line) used in our experiments and use this to extrapolate the O_2 concentration expected for much longer electrodes (dashed orange line). The O_2 concentration decreases significantly along a 50 cm long electrode and results in an outlet concentration of only 0.1 mM, versus an inlet concentration of 1.1 mM. The ORR current density is highly dependent on the local O_2 concentration and will thus decrease accordingly higher up in the channel. In turn, O_2 depletion along the electrolyzer channel lowers the average geometric current density (Figure 7b). Therefore, even a system with perfect selectivity will be limited by the amount of O_2 as it is scaled up.

Increasing the flow velocity improves the situation considerably in terms of preventing O_2 depletion along the channel (Figure 7a) and results in a higher average geometric current density (Figure 7b). The higher flow velocity increases the limiting current density in two ways; first, the higher flow rate supplies more fresh electrolyte, which keeps the O_2 concentration high. Second, the higher flow velocity increases the mass transfer coefficient. Despite this double effect, the gain in local O_2 concentration and average current density is the largest at relatively low flow velocities. This follows from the exponential term in eq 11, representing the limit of fresh electrolyte (i.e., the limited inflow concentration). As an example, increasing the flow velocity from 19 to 100 mm/s raises the minimum O_2 concentration 5 times and doubles the average current density, while increasing the flow velocity to 600 mm/s (a factor 30 higher than 19 mm/s) increases the

https://doi.org/10.1021/acssuschemeng.4c03919
ACS Sustainable Chem. Eng. 2024, 12, 12909−12918

current density only 4 times and induces a significant pressure drop.

The balance between the increased performance and increased pumping costs with the increased flow velocity should be optimized in any electrochemical flow system. As a result, typical flow velocities in comparable applications with single phase flow, such as electrodialysis, are in the order of 10−150 mm/s.[29] The j_{avg}−curve in Figure 7b is also steepest in this region, and we expect similar flow velocities to be relevant in our flow-through system, with the most favorable trade-off between increased geometric current density and pumping costs in this regime. We estimated that the theoretical pumping power is already 34% of the electrochemical power at a flow velocity of 600 mm/s in a single-pass (calculation in Supporting Information), which makes it unpractical to flow at such high velocities.

In addition, the electrolyte flow velocity and current density control the H_2O_2 concentration in the product stream and will influence the choice between designing an electrolyte recycling system or a single-pass system. High flow velocities would require a recycling system in order to achieve a sufficiently high H_2O_2 concentration, but will allow for O_2-resaturation and maintain higher O_2 concentrations along with the increasing H_2O_2 concentration. Lower flow velocities will be necessary in a single-pass system, but such a system will have to cope with decreasing the O_2 concentration during the same H_2O_2 concentration increase needed to satisfy application requirements. Therefore, the electrode height and flow velocity should be optimized to fit the current density and system requirements as well.[20,30] Alternatively, the inlet O_2 concentration can be increased by pressurizing the system, or options for in-channel saturation, such as bubbling O_2 directly into the reaction channel, could be investigated.

Although the low O_2 solubility remains a challenge in any aqueous system, the flow-through configuration allows for higher current densities and thicker channels with larger total amounts of available O_2 compared to a flow-by configuration, while avoiding stability issues in GDEs due to salt formation,[31] flooding,[32] and water management in general.[33,34] Even so, flow-through and GDE configurations are promising concepts to solve the limitation of the O_2 mass transfer, each with their own advantages and drawbacks. Although the stability issues in GDEs need to be considered, GDEs provide better O_2 availability in the entire channel compared to a flow-through system, whereas the flow-through system might offer easier scalability and higher stability due to the more simple and robust system design.

CONCLUSIONS

We electrochemically produced H_2O_2 via the two-electron ORR with Cu-tmpa as a homogeneous catalyst at neutral pH in an electrochemical flow cell with different electrode configurations. We achieved similar Faradaic efficiencies for H_2O_2 to previously studied RDE systems with the Cu-tmpa catalyst, while the electrode area can be extended in flow cells. This indicates that this is a promising way of scaling up this reaction. We achieved the highest current density and H_2O_2 concentration in a flow-through configuration. The limiting current density was improved 10−25 times in the flow-through compared to the flow-by configuration due to the larger electrode area and due to higher mass transfer coefficients in flow-through electrodes. The electrode configuration had a significantly larger effect on the limiting current than the electrolyte flow rate; the flow velocity has only a minor effect when using a small (3.4 cm long) flow-through electrode. The high current density in flow-through electrodes was paired with increased difficulties in maintaining the initial current density and FE during CA. The higher O_2 consumption- and H_2O_2 production rates shifted the $[O_2]/[H_2O_2]$ ratio in favor of H_2O_2 reduction and increased the competition between O_2 and H_2O_2 reduction over time. Although this resulted in the most severe performance drop in the flow-through configuration, the H_2O_2 production rate remains the highest in this configuration, and the H_2O_2 concentration entered the mM range. In contrast, the suspension electrodes, which have an even higher contact area with the liquid phase, did not yield any detectable H_2O_2. We showed that any H_2O_2 that may be produced will be immediately decomposed by the AC material, rendering this particular carbon material unsuitable for the ORR to H_2O_2.

We have demonstrated that implementing a flow-through principle in an ORR flow system can greatly reduce mass transfer limitations already at low electrolyte flow and boost H_2O_2 production rates, enabling us to produce meaningful H_2O_2 concentrations in a neutral solution with Cu-tmpa as the ORR catalyst. Although the availability of O_2 is greatly improved on the microscale, it will decrease through the height of the channel and cause difficulties when scaling to larger flow cells. Here, increasing the flow rate will have a larger positive effect than that in the small flow cell used in the experiments. Future studies should apply a fast O_2 saturation method to ensure the maximum O_2 concentration at the channel inlet and carefully design the electrode height, flow velocity, and recirculation ratio to suit the current density in the electrochemical H_2O_2 synthesis systems.

ASSOCIATED CONTENT

Supporting Information

The Supporting Information is available free of charge at https://pubs.acs.org/doi/10.1021/acssuschemeng.4c03919.

Schematic of ORR flow cell and setup; detailed description of electrochemical analysis; additional CV scans of suspension electrodes; calculation of overall O_2 depletion over time; used method for estimating limiting currents and predicting them from Sherwood correlations; and estimation of pressure drop in the flow-through system (relevant data available in the Zenodo repository at 10.5281/zenodo.12622235) (PDF)

AUTHOR INFORMATION

Corresponding Author

David A. Vermaas − *Department of Chemical Engineering, Delft University of Technology, 2629HZ Delft, The Netherlands;* orcid.org/0000-0002-4705-6453; Email: D.A.Vermaas@tudelft.nl

Authors

Nathalie E.G. Ligthart − *Department of Chemical Engineering, Delft University of Technology, 2629HZ Delft, The Netherlands;* orcid.org/0009-0004-5594-2190

Phebe H. van Langevelde − *Leiden Institute of Chemistry, Leiden University, 2333 CC Leiden, The Netherlands*

Johan T. Padding − *Department of Process and Energy, Delft University of Technology, 2628 CB Delft, The Netherlands;* orcid.org/0000-0003-4161-0748

Dennis G.H. Hetterscheid − *Leiden Institute of Chemistry, Leiden University, 2333 CC Leiden, The Netherlands;* orcid.org/0000-0001-5640-4416

Complete contact information is available at: https://pubs.acs.org/10.1021/acssuschemeng.4c03919

Author Contributions

All authors have given approval to the final version of the manuscript.

Funding

This project has received funding from the European Research Council (ERC) from the ERC Proof of Concept grant 899535 Cu4Peroxide to D. G. H. H. and under the European Union's Horizon 2020 research and innovation program (Grant agreement No. 852115). This work reflects the authors' view, and the ERC Executive Agency is not responsible for any use resulting from the information it contains.

Notes

The authors declare no competing financial interest.

REFERENCES

(1) Noyori, R.; Aoki, M.; Sato, K. Green oxidation with aqueous hydrogen peroxide. *Chem. Commun.* **2003**, 1977−1986.
(2) McDonnell, G. The Use of Hydrogen Peroxide for Disinfection and Sterilization Applications. In *Patai's Chemistry of Functional Groups*; John Wiley & Sons, Ltd,: 2014; pp 1−34.
(3) Hage, R.; Lienke, A. Applications of Transition-Metal Catalysts to Textile and Wood-Pulp Bleaching. *Angew. Chem., Int. Ed.* **2006**, *45*, 206−222.
(4) Fast, S. A.; Gude, V. G.; Truax, D. D.; Martin, J.; Magbanua, B. S. A Critical Evaluation of Advanced Oxidation Processes for Emerging Contaminants Removal. *Environmental Processes* **2017**, *4*, 283−302.
(5) Zhang, X.; Xia, Y.; Xia, C.; Wang, H. Insights into Practical-Scale Electrochemical H2O2 Synthesis. *Trends in Chemistry* **2020**, *2*, 942−953.
(6) Campos-Martin, J. M.; Blanco-Brieva, G.; Fierro, J. L. G. Hydrogen Peroxide Synthesis: An Outlook beyond the Anthraquinone Process. *Angew. Chem., Int. Ed.* **2006**, *45*, 6962−6984.
(7) Ciriminna, R.; Albanese, L.; Meneguzzo, F.; Pagliaro, M. Hydrogen Peroxide: A Key Chemical for Today's Sustainable Development. *ChemSusChem* **2016**, *9*, 3374−3381.
(8) Dan, M.; et al. Strategies and challenges on selective electrochemical hydrogen peroxide production: Catalyst and reaction medium design. *Chem. Catalysis* **2022**, *2*, 1919−1960.
(9) An, J.; et al. Electrosynthesis of H2O2 through a two-electron oxygen reduction reaction by carbon based catalysts: From mechanism, catalyst design to electrode fabrication. *Environmental Science and Ecotechnology* **2022**, *11*, No. 100170.
(10) Pérez, J. F.; et al. Towards the scale up of a pressurized-jet microfluidic flow-through reactor for cost-effective electro-generation of H2O2. *Journal of Cleaner Production* **2019**, *211*, 1259−1267.
(11) Berl, E. A New Cathodic Process for the Production of H2O2. *Transactions of The Electrochemical Society* **1939**, *76*, 359.
(12) Wang, N.; Ma, S.; Zuo, P.; Duan, J.; Hou, B. Recent Progress of Electrochemical Production of Hydrogen Peroxide by Two-Electron Oxygen Reduction Reaction. *Advanced Science* **2021**, *8*, No. 2100076.
(13) Langerman, M.; Hetterscheid, D. G. H. Mechanistic Study of the Activation and the Electrocatalytic Reduction of Hydrogen Peroxide by Cu-tmpa in Neutral Aqueous Solution. *ChemElectroChem.* **2021**, *8*, 2783−2791.
(14) Langerman, M.; Hetterscheid, D. G. H. Fast Oxygen Reduction Catalyzed by a Copper(II) Tris(2-pyridylmethyl)amine Complex through a Stepwise Mechanism. *Angew. Chem., Int. Ed.* **2019**, *58*, 12974−12978.
(15) van Langevelde, P. H.; Hetterscheid, D. G. H. Selective Electrochemical H2O2 Production by a Molecular Copper Catalyst: A Crucial Relation between Reaction Rate and Mass Transport. *Chem. Catal.* **2024**, No. 101069.
(16) Zhang, C.; et al. Three-dimensional electrochemical process for wastewater treatment: A general review. *Chemical Engineering Journal* **2013**, *228*, 455−467.
(17) Mourshed, M.; et al. Carbon-based slurry electrodes for energy storage and power supply systems. *Energy Storage Materials* **2021**, *40*, 461−489.
(18) Rommerskirchen, A.; et al. Unraveling charge transport in carbon flow-electrodes: Performance prediction for desalination applications. *Carbon* **2019**, *145*, 507−520.
(19) Ligthart, N. E. G.; Prats Vergel, G.; Padding, J. T.; Vermaas, D. A. Practical potential of suspension electrodes for enhanced limiting currents in electrochemical CO2 reduction. *Energy Adv.* **2024**, *3*, 841.
(20) Li, W.; Bonakdarpour, A.; Gyenge, E.; Wilkinson, D. P. Production of Hydrogen Peroxide for Drinking Water Treatment in a Proton Exchange Membrane Electrolyzer at Near-Neutral pH. *J. Electrochem. Soc.* **2020**, *167*, No. 044502.
(21) Young, M. N.; Links, M. J.; Popat, S. C.; Rittmann, B. E.; Torres, C. I. Tailoring Microbial Electrochemical Cells for Production of Hydrogen Peroxide at High Concentrations and Efficiencies. *ChemSusChem* **2016**, *9*, 3345−3352.
(22) Parsons, R. *Electrochemical nomenclature.* **1974**, *37*, 499−516.
(23) Weusten, S. J. C.; Murrer, L. C. E. M.; de Groot, M. T.; van der Schaaf, J. Mass transfer in 3D-printed electrolyzers: The importance of inlet effects. *AIChE J.* **2021**, *67*, No. e17263.
(24) Choo, K. Y.; Yoo, C. Y.; Han, M. H.; Kim, D. K. Electrochemical analysis of slurry electrodes for flow-electrode capacitive deionization. *J. Electroanal. Chem.* **2017**, *806*, 50−60.
(25) Wen, Y.; et al. Electrochemical Reactors for Continuous Decentralized H2O2 Production. *Angew. Chem., Int. Ed.* **2022**, *61*, No. e202205972.
(26) Akuzum, B.; et al. Percolation Characteristics of Conductive Additives for Capacitive Flowable (Semi-Solid) Electrodes. *ACS Appl. Mater. Interfaces* **2020**, *12*, 5866−5875.
(27) Boota, M.; Hatzell, K. B.; Alhabeb, M.; Kumbur, E. C.; Gogotsi, Y. Graphene-containing flowable electrodes for capacitive energy storage. *Carbon* **2015**, *92*, 142−149.
(28) Gunn, D. J. Transfer of heat or mass to particles in fixed and fluidised beds. *Int. J. Heat Mass Transfer* **1978**, *21*, 467−476.
(29) Ankoliya, D.; et al. Design and optimization of electrodialysis process parameters for brackish water treatment. *Journal of Cleaner Production* **2021**, *319*, No. 128686.
(30) Pangotra, D.; Csepei, L.-I.; Roth, A.; Sieber, V.; Vieira, L. Anodic generation of hydrogen peroxide in continuous flow. *Green Chem.* **2022**, *24*, 7931−7940.
(31) Lees, E. W.; Mowbray, B. A. W.; Parlane, F. G. L.; Berlinguette, C. P. Gas diffusion electrodes and membranes for CO2 reduction electrolysers. *Nature Reviews Materials* **2022**, *7*, 55−64.
(32) Yang, K.; Kas, R.; Smith, W. A.; Burdyny, T. Role of the Carbon-Based Gas Diffusion Layer on Flooding in a Gas Diffusion Electrode Cell for Electrochemical CO2 Reduction. *ACS Energy Letters* **2021**, *6*, 33−40.
(33) De Mot, B.; Hereijgers, J.; Duarte, M.; Breugelmans, T. Influence of flow and pressure distribution inside a gas diffusion electrode on the performance of a flow-by CO2 electrolyzer. *Chemical Engineering Journal* **2019**, *378*, No. 122224.
(34) Baumgartner, L. M.; Koopman, C. I.; Forner-Cuenca, A.; Vermaas, D. A. Narrow Pressure Stability Window of Gas Diffusion Electrodes Limits the Scale-Up of CO2 Electrolyzers. *ACS Sustainable Chem. Eng.* **2022**, *10*, 4683−4693.